

## Leucite at high pressure: Elastic behavior, phase stability, and petrological implications

G. DIEGO GATTA,<sup>1,2,\*</sup> NICOLA ROTIROTI,<sup>1,2</sup> TIZIANA BOFFA BALLARAN,<sup>3</sup> AND ALESSANDRO PAVESE<sup>1,2</sup>

<sup>1</sup>Dipartimento di Scienze della Terra, Università degli Studi di Milano, Via Botticelli 23, I-20133 Milano, Italy

<sup>2</sup>CNR-Istituto per la Dinamica dei Processi Ambientali, Milano, Italy

<sup>3</sup>Bayerisches Geoinstitut, Universitaet Bayreuth, Universitaetsstrasse 30, D-95447 Bayreuth, Germany

### ABSTRACT

Elastic and structural behavior of a natural tetragonal leucite from the volcanic Lazio district (Italy) were investigated at high pressure by in situ single-crystal X-ray diffraction with a diamond anvil cell under hydrostatic conditions. A first-order phase transition, never reported in the literature, was observed at  $P = 2.4 \pm 0.2$  GPa from tetragonal ( $I4_1/a$ ) to triclinic symmetry (analysis of diffraction intensities suggests the space group  $P\bar{1}$ ), accompanied by a drastic increase in density of about 4.7%. The transition pressure was bracketed by several measurements in compression and decompression. No further phase-transition has been observed up to 7 GPa. Fitting a second-order Birch-Murnaghan equation of state (BM-EoS) to the pressure-volume data of the tetragonal polymorph, we obtain  $K_0 = 41.9(6)$  GPa and  $K' = 4$  (fixed). In the case of the triclinic polymorph, a second-order BM-EoS gives  $K_0 = 33.2(5)$  GPa. The eulerian finite strain ( $f_e$ ) vs. normalized stress ( $F_e$ ) curves were calculated for the low- and high- $P$  polymorphs, providing  $F_e(0) = 42(1)$  and  $F_e(0) = 33.2(4)$  GPa, respectively. The axial bulk modulus values of the tetragonal polymorph, calculated with a linearized BM-EoS, are  $K_0(a) = 34.5(5)$  and  $K_0(c) = 78(1)$  GPa. For the triclinic polymorph, we obtain  $K_0(a) = 35.9(5)$ ,  $K_0(b) = 34.9(7)$ , and  $K_0(c) = 35.5(7)$  GPa. The elastic behavior of the low- $P$  polymorph appears to be more anisotropic than that of the high- $P$  polymorph. The HP-crystal structure evolution of the tetragonal polymorph of leucite was studied on the basis of six structural refinements at different pressures between 0.0001 and 1.8 GPa. The main deformation mechanisms at high-pressure are due to tetrahedral tilting, giving rise to an increase of the ellipticity of the four- and six-membered rings of the tetrahedral framework. The T-O bond distances are practically invariant within the stability field of the tetragonal polymorph. The complex  $P$ -induced twinning, due to the tetragonal  $\rightarrow$  triclinic phase-transition, and the low quality of the diffraction data at pressure above the phase-transition, did not allow the refinement of the crystal structure of the triclinic polymorph.

**Keywords:** Leucite, single-crystal X-ray diffraction, high pressure, compressibility, phase transition

### INTRODUCTION

Leucite is commonly defined as a feldspathoid, with ideal formula  $K_{16}Al_{16}Si_{32}O_{96}$ , although the Commission of the International Mineralogical Association attributed leucite to the zeolite group (Coombs et al. 1997), mainly because of the structural homologies with analcime. Leucite occurs as a primary mineral in volcanic rocks, especially potassium-rich mafic and ultramafic rocks [e.g., leucite-basanites, leucite-tephrites, leucite-phonolites, leucite-melilite basalts, ugandites, and katungites (Peccerillo 1998, 2003, 2005; Deer et al. 2004)].

Leucite is isotypic with analcime (Gottardi and Galli 1985; Armbruster and Gunter 2001; Baerlocher et al. 2001). The crystal structure of open-framework silicates belonging to the “analcime group” [analcime  $Na_{16}Al_{16}Si_{32}O_{96} \cdot 16H_2O$ , leucite, wairakite  $Ca_8Al_{16}Si_{32}O_{96} \cdot 16H_2O$ , pollucite  $Cs_{12}Na_4Al_{16}Si_{32}O_{96} \cdot 12H_2O$ , and hsianghualite  $Li_{16}Ca_{24}Be_{24}Si_{24}O_{96}F_{16}$  (Armbruster and Gunter 2001)] results from the combination of two “secondary building units” (SBU), consisting of four- and six-membered rings

of tetrahedra, as shown in Figure 1 (Baerlocher et al. 2001). The framework topology of this group of minerals (i.e., ANA topology) shows the maximum symmetry ( $Ia\bar{3}d$ , Baerlocher et al. 2001). In leucite, the extra-framework content is represented only by K, which is located at the same site occupied by  $H_2O$  in the analcime structure, forming a distorted polyhedron with six K-O bond distances between 2.96 and 3.14 Å and six distances between 3.50 and 3.76 Å (Mazzi et al. 1976).

All crystals of natural leucite grow as cubic crystals at natural conditions ( $T > 900$  °C), with space group  $Ia\bar{3}d$  and  $a \approx 13.54$  Å (Faust 1963; Peacor 1968; Taylor and Henderson 1968; Mazzi et al. 1976; Palmer et al. 1989, 1990, 1997). With decreasing temperature, leucite undergoes two phase transitions between 600 and 700 °C with a reduction of symmetry from cubic to tetragonal (high- $T$ :  $Ia\bar{3}d \rightarrow I4_1/acd$ ; low- $T$ :  $I4_1/acd \rightarrow I4_1/a$ ). The two phase transitions are displacive and lead to large spontaneous strains (Palmer et al. 1989, 1997). A recent calorimetric study performed by Newton et al. (2008), interpreted with Landau theory, showed that the thermodynamic character of both the aforementioned  $T$ -induced phase-transitions in leucite is near-tricritical, with  $T_{TR-1} \approx 646$  °C (and  $T_{C1} \approx 644.9$  °C) and  $T_{TR-2} \approx$

\* E-mail: diego.gatta@unimi.it

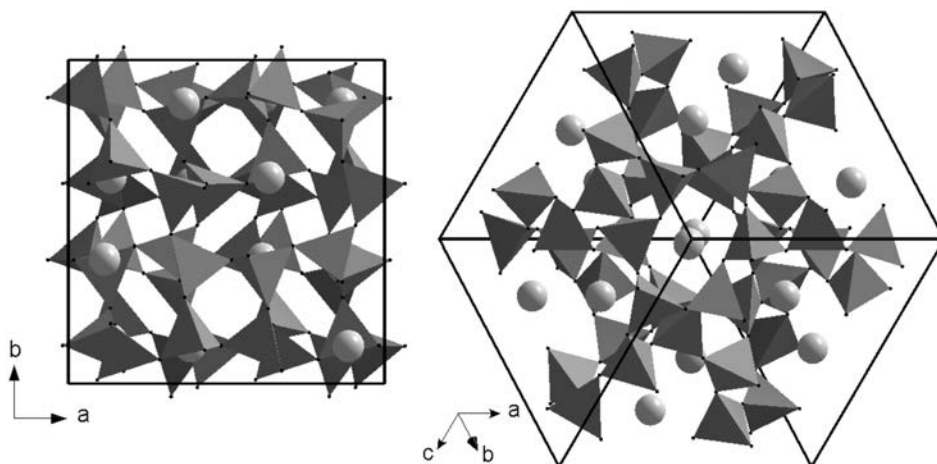


**FIGURE 1.** The crystal structure of leucite viewed down  $[001]$  and  $[\bar{1}\bar{1}\bar{1}]$ . The large spheres represent the extra-framework potassium sites.

627 °C (and  $T_{c2} \approx 634$  °C).

At room temperature, leucite is tetragonal (with space group  $I4_1/a$ ,  $a \approx 13.07$ ,  $c \approx 13.75$  Å, Mazzi et al. 1976). Due to the phase-transition from cubic to tetragonal symmetry, complex twins are formed, since all six planes of the cubic form  $\{110\}$  may become twin planes in the tetragonal polymorph (with point group  $4/m$ ). On the basis of optical observations and single-crystal X-ray diffraction, Mazzi et al. (1976) reported two common cases found in natural leucite: (1) merohedric twins develop on the tetragonal planes (110) and  $(\bar{1}\bar{1}0)$  (with the two individuals having parallel crystallographic axes, but with  $a$  and  $b$  interchanged), and (2) pseudo-merohedric twins develop on the tetragonal planes (101), (011),  $(\bar{1}01)$ , and  $(0\bar{1}1)$  [with the two individuals having parallel  $a$  (or  $b$ ) axes, but the remaining two axes not being parallel]. The complex twinning in natural leucite was also investigated by Palmer et al. (1988) using X-ray precession photos and TEM diffraction patterns and images.

For both high- $T$  cubic and low- $T$  tetragonal forms, no Si/Al-ordering in the tetrahedral framework was found (Peacor 1968; Mazzi et al. 1976; Brown et al. 1987; Palmer et al. 1997). The leucite structure hosts ionic substitution, and compounds in the system  $KAlSi_2O_6$ - $RbAlSi_2O_6$ - $CsAlSi_2O_6$  have been synthesized. A relationship between the ionic radius of the extra-framework cation and the transition temperature for the tetragonal/cubic phase transition was found by Taylor and Henderson (1968). The thermo-elastic behavior and the  $T$ -induced structural evolution of natural, synthetic and Rb- and Cs-bearing leucite has been extensively investigated using different techniques (Faust 1963; Peacor 1968; Taylor and Henderson 1968; Hirao et al. 1976; Lange et al. 1986; Palmer et al. 1989, 1990, 1997; Boysen 1990; Heaney and Veblen 1990; Hatch et al. 1990; Dove et al. 1993).

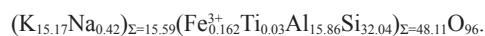
The HP behavior of a synthetic leucite was investigated by means of synchrotron X-ray powder diffraction up to 5.1 GPa by Fasshauer et al. (1998). The authors reported only the  $P$ - $V$  data and no structural refinement at high pressure was performed. No phase transition was found within the  $P$  range investigated. Fasshauer et al. (1998) calculated the bulk modulus of leucite and its  $P$ -derivative using a Murnaghan Equation-of-State (EoS, Murnaghan 1937), obtaining  $K_0 = 45$  GPa and  $K' = 5.7$ . However, the  $P$ - $V$  data are significantly scattered and do not provide clear

evidence of phase-stability of the tetragonal leucite within the pressure range investigated.

In the wake of previous experiments on the HP behavior of the isotopic analcime (Gatta et al. 2006) and wairakite (Ori et al. 2008), which show a  $P$ -induced phase-transition, one could expect similar behavior also in leucite. The aim of this study is to investigate the elastic behavior and  $P$ -induced structural evolution of a natural leucite specimen by in situ HP single-crystal X-ray diffraction with a diamond anvil cell. The precision and accuracy of single-crystal data allow a reliable description of the elastic behavior of leucite and the detection of any possible  $P$ -induced phase-transformation.

## EXPERIMENTAL METHODS

A sample of natural leucite (labeled CR-8) from the potassium-rich lavas of the Sabatini volcanic district, Roman co-magmatic Province (Lazio, Italy), associated to the Plio-Quaternary volcanism (Conticelli and Peccerillo 1992; Conticelli et al. 2002; Peccerillo 1998, 2003, 2005; Federico et al. 1994), was used for the high-pressure experiments. Quantitative chemical analyses in EMPA-WDS mode were performed on a polished single crystal, optically free of defects, using a Jeol JXA-8200 electron microprobe at the laboratory of the Earth Sciences Department, University of Milan (ESD-MI). The system was operated using a defocused electron beam ( $\varnothing$  5  $\mu$ m) at an accelerating voltage of 15 kV, a beam current of 15 nA and a counting time of 20 s on the peaks and 5 s on the backgrounds. Natural minerals (K-feldspar for Si, K, Al; forsterite for Mg; wollastonite for Ca; omphacite for Na; ilmenite for Ti; fayalite for Fe) were employed as standards. The results were corrected for matrix effects using a conventional ZAF routine in the Jeol suite of programs. The crystal was found to be homogeneous within the analytical error. The chemical content (obtained by averaging four points analyses) is  $Na_2O$  0.38%,  $K_2O$  20.51%,  $CaO$  <0.01%,  $MgO$  <0.01%,  $Fe_2O_3$  0.37 wt%,  $TiO_2$  0.07 wt%,  $Al_2O_3$  23.25%,  $SiO_2$  55.28% (Total: 99.85 wt%). The chemical formula, on the basis of 96 O atoms, is



The majority of the crystals of leucite from the natural sample used in our experiments showed evidence of pseudo-merohedric twinning on the optical scale; this class of crystals is not ideal for diffraction experiments (Mazzi et al. 1976). A platy crystal of leucite ( $180 \times 140 \times 60$   $\mu$ m<sup>3</sup>), free of defects and without any evidence of pseudo-merohedric twinning on the optical scale, was selected for the X-ray diffraction experiments. Diffraction intensity data were first collected at room conditions with an Oxford Diffraction-Xcalibur-1 diffractometer equipped with a CCD, using a graphite monochromator for  $MoK\alpha$ -radiation, operated at 50 kV and 40 mA. A combination of  $\omega$  and  $\varphi$  scans was used to maximize the reciprocal space coverage (and redundancy), fixing a step size of 0.4°, a time of 10 s/frame (Table 1) and a crystal-detector distance of 80 mm. A total of 52 805 Bragg reflex-

**TABLE 1.** Details pertaining to the data collection and structural refinements of tetragonal leucite at different pressures

<i>P</i> (GPa)	0.0001	0.0001*	0.38(5)	1.20(5)	1.77(5)	0.0001†
Crystal size (μm <sup>3</sup> )	180 × 140 × 60	180 × 140 × 60	180 × 140 × 60	180 × 140 × 60	180 × 140 × 60	180 × 140 × 60
<i>a</i> (Å)	13.084(1)	13.097(4)	13.053(4)	12.955(5)	12.891(5)	13.073(2)
<i>c</i> (Å)	13.784(2)	13.755(4)	13.732(4)	13.684(5)	13.653(5)	13.731(3)
<i>T</i> (K)	298	298	298	298	298	298
Radiation	MoKα	MoKα	MoKα	MoKα	MoKα	MoKα
Detector type	CCD	PD	PD	PD	PD	PD
2θ range (°)	2–60	2–60	2–60	2–60	2–60	2–60
Scan type	ω/φ	ω	ω	ω	ω	ω
Scan speed (°/s)	–	0.02	0.02	0.02	0.02	0.02
Time per frame (s)	10	–	–	–	–	–
Scan width (°)	0.4	1.4	1.4	1.4	1.4	1.4
Space group	<i>I</i> <sub>4</sub> / <i>a</i>					
No. measured reflections with <i>F</i> <sub>0</sub> > 4σ( <i>F</i> <sub>0</sub> )	18892	474	471	468	457	3708
No. unique reflections with <i>F</i> <sub>0</sub> > 4σ( <i>F</i> <sub>0</sub> )	1026	226	221	215	202	1325
No. refined parameters	93	36	36	36	36	93
<i>R</i> <sub>int</sub>	0.075	0.0965	0.1216	0.1285	0.1214	0.0541
<i>R</i> <sub>1</sub> ( <i>F</i> ) with <i>F</i> <sub>0</sub> > 4σ( <i>F</i> <sub>0</sub> )	0.0573	0.0788	0.0784	0.0743	0.0773	0.0449
<i>wR</i> <sub>2</sub> ( <i>F</i> <sup>2</sup> )	0.1366	0.1530	0.1581	0.1601	0.1659	0.0993
Goof	1.271	1.084	1.049	1.077	1.071	1.149
Residuals (e <sup>-</sup> /Å <sup>3</sup> )	+0.58/–0.63	+0.49/–0.59	+0.53/–0.51	+0.52/–0.61	+0.44/–0.48	+0.88/–0.58

Notes: Standard deviations are in parentheses.  $R_{\text{int}} = \sum |F_{\text{obs}}^2 - F_{\text{calc}}^2| / \sum F_{\text{obs}}^2$ ;  $R_1 = \sum (|F_{\text{obs}}| - |F_{\text{calc}}|) / \sum |F_{\text{obs}}|$ ;  $wR_2 = \{ \sum [w(F_{\text{obs}}^2 - F_{\text{calc}}^2)]^2 / \sum [w(F_{\text{obs}}^2)]^2 \}^{0.5}$ .

\* Crystal in the DAC, without *P*-medium.

† Crystal in air after decompression.

tions was collected in the range  $2 < 2\theta < 60^\circ$ , of which 1026 were unique with  $F_0 > 4\sigma(F_0)$  (Table 1), giving a metrically tetragonal lattice with  $a = 13.084(1)$  and  $c = 13.784(2)$  Å (Table 1). An inspection of the diffraction pattern showed evidence of weak pseudo-merohedric twinning. The diffraction data belonging to the pseudo-merohedric individual were not integrated. After *Lp* and empirical absorption corrections by Gaussian integration based upon the physical description of the crystal (CrysAlis, Oxford Diffraction 2005), the discrepancy factor between symmetry related diffraction intensities (Laue class *4/m*) was  $R_{\text{int}} \approx 0.075$  (Table 1). The reflection conditions were consistent with space group *I*<sub>4</sub>/*a* (Mazzi et al. 1976). The structural refinement was performed with anisotropic displacement parameters using the SHELX-97 software (Sheldrick 1997), starting from the atomic coordinates of Mazzi et al. (1976). Neutral atomic scattering factors of K, Si, and O from the *International Tables for Crystallography* (Wilson and Prince 1999) were used. A scattering curve based on mixed occupancy of tetrahedral sites (by Al and Si) did not improve significantly the refinement figures of merit. A correction for the effects due to the merohedric twin was applied, and the refined volume values of the two individuals resulted 60 and 40%. The convergence was rapidly achieved after a few cycles of refinement. At the end of the refinement, no peak larger than  $+0.58/-0.63$  e<sup>-</sup>/Å<sup>3</sup> was observable in the final difference Fourier synthesis, and  $R_1(F) \approx 0.05$  for 93 refined parameters. Further details of the structure refinement are reported in Table 1. Refined atomic positions and displacement parameters are listed in Table 2. Bond distances (Table 3) and angles are consistent with a disordered Si/Al-distribution in the tetrahedral framework (Mazzi et al. 1976).

An ETH-type diamond anvil cell (DAC, Miletich et al. 2000) was used for the high-pressure experiments at room *T*. Steel T301 foil, 250 μm thick, was used as a gasket. The gasket foil was pre-indented to a thickness of about 110 μm before drilling a micro-hole (Ø 350 μm) by spark-erosion. The crystal of leucite previously studied at room conditions was placed into the gasket hole together with a single-crystal of quartz used for the pressure calibration (Angel et al. 1997). A methanol:ethanol (4:1) mixture was used as hydrostatic pressure-transmitting medium (Angel et al. 2007). Accurate lattice parameters were determined at pressures ranging between 0.0001 and 4.32 GPa (Table 4) with a KUMA-KM4 diffractometer, equipped with a point-detector and a monochromatized MoKα-radiation, on the basis of 24 Bragg reflections. Intensity data used for the structure refinements at pressures (GPa) of 0.0001 (with crystal in DAC without any pressure medium), 0.38, 1.20, 1.77, and at 0.0001 (with the crystal in air) after decompression were collected, adopting the data collection strategy reported in Table 1. No violation of the reflection conditions for *I*<sub>4</sub>/*a* symmetry was observed in any data collection. Integrated intensity data were corrected for *Lp* and absorption effects due to the crystal and the DAC using the ABSORB5.2 computer program (Burnham 1966; Angel 2002, 2003). The HP-structure refinements were performed with isotropic displacement parameters. To reduce the number of the refined variables, the displacement parameters were refined by grouping those of the T and O sites (Table 2). Geometrical soft restraints were used to restrain the T-O bond distances to a reference value of 1.65 Å with an estimated standard deviation of ±0.02 Å. Refined atomic positions, displacement parameters and bond distances at high

pressure are reported in Tables 2 and 3. A first-order phase transition occurred at about 2.4 GPa, well evident in transmitted polarized light and on the basis of the lattice parameters, from tetragonal to triclinic symmetry. The lattice metric was confirmed by diffraction data collected with a diffractometer equipped with a CCD. The quality of the diffraction data, the complexity of the *P*-induced twinning due to the tetragonal → triclinic phase-transition and the larger number of parameters necessary to describe the new phase did not allow refinement of the crystal structure of the HP triclinic polymorph; thus only the unit-cell constants at different pressures were measured (Table 4).

A further HP experiment was performed with a new crystal of the CR-8 leucite (150 × 120 × 60 μm<sup>3</sup>) at the Bayerisches Geoinstitut-Bayreuth (BGI), adopting the same DAC and *P*-medium used in the previous HP-experiment. Accurate lattice parameters were measured up to about 7 GPa (Table 4) with a Huber four-circle diffractometer (non-monochromatized MoKα radiation) using eight-position centering of 18 Bragg reflections, according to the protocol of King and Finger (1979) and Angel et al. (2000).

## RESULTS: ELASTIC BEHAVIOR AND PHASE-STABILITY

The evolution of the lattice parameters of leucite with pressure, measured at the ESD-MI and at the BGI, is shown in Figure 2. A first-order phase transition is observed in the pressure range between 2.2 and 2.6 GPa. The transition pressure was bracketed by several measurements in compression and decompression. The HP-polymorph shows a metrically triclinic lattice, describable as a distortion of the tetragonal one with  $a \approx b \approx c$  and  $\beta > \alpha \approx \gamma$  (Table 4). The tetragonal → triclinic phase transition is reversible and without any appreciable hysteresis effect. Optical and diffraction observations show that the phase-transition gives rise to complex twinning of the crystal. As shown in Figure 2, the evolution of the unit-cell constants with *P* is continuous and monotonic up to 6.98 GPa, without any evidence of a further phase-transition or anomalous elastic behavior within the *P*-range investigated.

The *P*-*V* data of the low- and high-*P* polymorphs were fitted with a second-order Birch-Murnaghan Equation-of-State (II-BM-EoS) (Birch 1947), using the EOS-FIT5.2 computer program (Angel 2001), using the data collected at the ESD-MI and at the BGI normalized to the room conditions values (i.e.,  $V/V_0$ ). The elastic parameters obtained, with the data weighted by the uncertainties in *P*-*V*, are the following:  $(V/V_0)_{P_0} = 1.0000(1)$ ,  $K_0$

**TABLE 2.** Refined atomic positions and displacement parameters ( $\text{\AA}^2$ ) of tetragonal leucite

Site	x	y	z	$U_{\text{eq}}/U_{\text{iso}}$
K (16f)	0.3659(2)	0.3643(2)	0.1144(2)	0.0642(7)
	0.36444(9)	0.3632(9)	0.1146(6)	0.063(3)
	0.3660(6)	0.3648(6)	0.1149(5)	0.052(2)
	0.3650(8)	0.3640(7)	0.1156(4)	0.050(3)
	0.3648(8)	0.3636(8)	0.1171(6)	0.043(3)
	0.36560(1)	0.3642(1)	0.1138(2)	0.0498(5)
T1 (16f)	0.0576(1)	0.3964(2)	0.1666(1)	0.0242(5)
	0.0586(6)	0.3966(6)	0.1668(4)	0.012(1)
	0.0569(5)	0.3970(5)	0.1669(4)	0.0094(8)
	0.0552(7)	0.3971(6)	0.1679(4)	0.011(1)
	0.0543(7)	0.3994(7)	0.1670(5)	0.012(1)
	0.0574(1)	0.3964(1)	0.1669(1)	0.0109(2)
T2 (16f)	0.1678(2)	0.6114(1)	0.1284(1)	0.0244(5)
	0.1683(6)	0.6101(7)	0.1281(4)	0.012(1)
	0.1690(4)	0.6105(4)	0.1273(4)	0.0094(8)
	0.1672(6)	0.6130(6)	0.1281(4)	0.011(1)
	0.1663(6)	0.6132(7)	0.1289(5)	0.012(1)
	0.1674(1)	0.6115(1)	0.1281(1)	0.0101(2)
T3 (16f)	0.3922(2)	0.6419(2)	0.0860(1)	0.0237(5)
	0.3925(6)	0.6417(6)	0.0870(4)	0.012(1)
	0.3926(5)	0.6414(5)	0.0864(4)	0.0094(8)
	0.3920(6)	0.6399(6)	0.0875(4)	0.011(1)
	0.3921(7)	0.6401(7)	0.0867(5)	0.012(1)
	0.3925(1)	0.6417(1)	0.08628(9)	0.0102(2)
O1 (16f)	0.1328(4)	0.3144(4)	0.1105(4)	0.040(1)
	0.1342(14)	0.3125(10)	0.1114(9)	0.020(2)
	0.1308(9)	0.3137(9)	0.1103(9)	0.016(2)
	0.1325(13)	0.3154(11)	0.1119(9)	0.016(2)
	0.1339(15)	0.3174(11)	0.1118(11)	0.019(2)
	0.1320(3)	0.3146(3)	0.1101(3)	0.0270(9)
O2 (16f)	0.0918(4)	0.5115(4)	0.1311(4)	0.036(1)
	0.0886(15)	0.5107(11)	0.1284(9)	0.020(2)
	0.0900(9)	0.5114(8)	0.1295(9)	0.016(2)
	0.0884(13)	0.5126(10)	0.1311(9)	0.016(2)
	0.0859(15)	0.5147(11)	0.1290(11)	0.019(2)
	0.0914(3)	0.5111(3)	0.1309(3)	0.0237(9)
O3 (16f)	0.1460(4)	0.6806(4)	0.2274(3)	0.032(1)
	0.1441(16)	0.6773(12)	0.2274(7)	0.020(2)
	0.1438(11)	0.6794(10)	0.2261(7)	0.016(2)
	0.1466(14)	0.6832(12)	0.2277(7)	0.016(2)
	0.1479(17)	0.6847(13)	0.2280(8)	0.019(2)
	0.1455(3)	0.6804(3)	0.2272(2)	0.0173(7)
O4 (16f)	0.1341(4)	0.6856(4)	0.0367(3)	0.036(1)
	0.1320(15)	0.6837(13)	0.0363(7)	0.020(2)
	0.1279(10)	0.6851(11)	0.0358(7)	0.016(2)
	0.1314(15)	0.6876(12)	0.0359(7)	0.016(2)
	0.1325(17)	0.6907(14)	0.0372(8)	0.019(2)
	0.1334(3)	0.6851(3)	0.0360(3)	0.0217(7)
O5 (16f)	0.2896(3)	0.5752(4)	0.1201(4)	0.032(1)
	0.2899(9)	0.5756(14)	0.1221(9)	0.020(2)
	0.2896(8)	0.5725(10)	0.1197(9)	0.016(2)
	0.2875(9)	0.5713(14)	0.1209(9)	0.016(2)
	0.2873(9)	0.5714(15)	0.1178(12)	0.019(2)
	0.2893(3)	0.5760(3)	0.1205(3)	0.0197(8)
O6 (16f)	0.4828(4)	0.6177(4)	0.1666(3)	0.031(1)
	0.4839(9)	0.6179(14)	0.1665(9)	0.020(2)
	0.4838(8)	0.6149(11)	0.1659(8)	0.016(2)
	0.4843(9)	0.6156(15)	0.1678(9)	0.016(2)
	0.4823(10)	0.6180(18)	0.1704(11)	0.019(2)
	0.4836(3)	0.6173(3)	0.1668(3)	0.0176(7)

Notes: For each site, values from top to bottom correspond to the refinement at 0.0001 GPa with the crystal in air; 0.0001 GPa with the crystal in the DAC; 0.38(5), 1.20(5), 1.77(5), and 0.0001 GPa with the crystal in air after decompression, respectively. For the refinements with the crystal in the DAC, the isotropic thermal parameters  $U_{\text{iso}}$  are reported, whereas for the refinements with the crystal in air  $U_{\text{eq}}$  are reported. Standard deviations are in parentheses.

= 41.9(6) GPa,  $K' = 4$  (fixed) for the low- $P$  tetragonal polymorph and  $(V/V_0)_{\text{P0}} = 0.986(1)$ ,  $K_0 = 33.2(5)$  GPa for the high- $P$  triclinic polymorph (Fig. 2).

The Eulerian finite strain, i.e.,  $f_e = [(V/V_0)^{2/3} - 1]/2$ , vs. normalized stress, i.e.,  $F_e = P/[3f(1 + 2f)^2]$ , curves for the low- and high- $P$  polymorphs were calculated using the more precise and

**TABLE 3.** Polyhedral bond distances ( $\text{\AA}$ ) and ellipticity of the 4mR-3, 6mR-1, and 6mR-2 of the tetragonal leucite at different pressures

P (GPa)	0.0001	0.0001*	0.38(5)	1.20(5)	1.77(5)	0.0001†
K-O5	2.936(5)	2.95(2)	2.89(1)	2.87(2)	2.86(2)	2.947(4)
K-O4	2.945(5)	2.98(2)	2.94(2)	2.90(2)	2.84(2)	2.952(4)
K-O3	2.977(5)	3.03(2)	2.97(1)	2.94(2)	2.93(2)	2.970(4)
K-O6	3.008(5)	3.01(2)	3.02(1)	2.99(2)	2.96(2)	2.993(4)
K-O2	3.024(5)	2.97(2)	3.00(2)	2.94(1)	2.88(2)	3.018(4)
K-O1	3.119(6)	3.09(2)	3.14(1)	3.08(2)	3.04(2)	3.127(5)
K-O1'	3.521(6)	3.54(2)	3.50(1)	3.50(2)	3.46(2)	3.509(5)
K-O5'	3.634(6)	3.60(2)	3.63(2)	(>3.59)	(>3.55)	3.610(5)
K-O4'	3.640(7)	3.61(2)	3.56(2)	3.58(2)	(>3.55)	3.631(6)
K-Si <sub>shortest</sub>	~3.64	~3.64	~3.64	~3.59	~3.55	~3.64
T1-O2	1.646(5)	1.633(11)	1.637(10)	1.637(12)	1.626(12)	1.640(4)
T1-O1	1.649(5)	1.642(12)	1.632(10)	1.626(10)	1.631(12)	1.648(4)
T1-O1'	1.649(5)	1.665(10)	1.6484(9)	1.647(11)	1.654(12)	1.644(4)
T1-O4	1.665(5)	1.657(11)	1.655(10)	1.630(11)	1.657(12)	1.646(4)
T2-O2	1.642(5)	1.668(12)	1.654(10)	1.654(12)	1.640(12)	1.646(4)
T2-O4	1.654(5)	1.658(13)	1.678(11)	1.655(12)	1.659(12)	1.650(4)
T2-O3	1.662(5)	1.656(12)	1.661(10)	1.660(12)	1.654(13)	1.657(3)
T2-O5	1.666(5)	1.657(12)	1.654(10)	1.653(12)	1.658(12)	1.663(4)
T3-O3	1.655(5)	1.643(11)	1.653(10)	1.664(11)	1.657(12)	1.650(3)
T3-O6	1.656(4)	1.652(11)	1.652(10)	1.654(11)	1.655(12)	1.656(3)
T3-O5	1.668(5)	1.670(12)	1.680(11)	1.683(12)	1.668(13)	1.667(4)
T3-O6'	1.670(5)	1.661(12)	1.669(10)	1.666(13)	1.677(12)	1.663(4)
$\epsilon_{4mR-3}$	0.9381(5)	0.9438(5)	0.9423(5)	0.9340(5)	0.9269(6)	0.9391(3)
$\epsilon_{6mR-1}$	0.674(2)	0.677(2)	0.6729(2)	0.670(2)	0.669(2)	0.675(1)
$\epsilon_{6mR-2}$	0.848(2)	0.850(3)	0.845(4)	0.846(3)	0.835(3)	0.848(1)

Note: Standard deviations are in parentheses.  $\epsilon_{4mR-3} = (T1-T3)/(T2-T2)$ ;  $\epsilon_{6mR-1} = (T2-T3)/(T3-T3)$ ;  $\epsilon_{6mR-2} = (T1-T1)_{\text{short}}/0.5[(T2-T2) + (T1-T1)_{\text{long}}]$ .

\* Crystal in the DAC, without  $P$ -medium.

† Crystal in air after decompression.

accurate data measured at the BGI. The  $f_e$ - $F_e$  plot is shown in Figure 3. The theoretical  $V_0$  values used for the Eulerian strains calculation pertaining to the HP-polymorph was calculated on the basis of the  $(V/V_0)_{\text{P0}}$  value refined with the II-BM-EoS and the measured  $V_0$  value at 0.0001 GPa [i.e.,  $V_0(f_e)_{\text{triclinic}} = (V/V_0)_{\text{P0-refined}} \cdot V_{0\text{-measured}} = 2317(3) \text{ \AA}^3$ ]. The weighted linear regressions through the data points give:  $F_e(0) = 42(1)$  GPa for the low- $P$  tetragonal polymorph and  $F_e(0) = 33.2(4)$  GPa for the high- $P$  triclinic polymorph. The  $f_e$ - $F_e$  plots, each with almost horizontal slope, are consistent with  $K' = 4$  for both the polymorphs.

The axial compressibility coefficients were calculated as “axial bulk moduli” [i.e.,  $K_{0j} = -1/(3\beta_j)$ ], where  $\beta_j$  is the axial compressibility coefficient] with a “linearized” BM-EoS (Angel 2000), simply substituting the cube of the lattice parameter for the volume. The elastic parameters for the low- $P$  tetragonal polymorph are  $(a/a_0)_{\text{P0}} = 0.99997(9)$  and  $K_0(a) = 34.5(5)$  GPa for the  $a$  axis and  $(c/c_0)_{\text{P0}} = 1.00003(7)$  and  $K_0(c) = 78(1)$  GPa for the  $c$  axis [ $K_0(a):K_0(b):K_0(c) = 1:1:2.26$ ]. For the high- $P$  triclinic polymorph, the linearized II-BM-EoS fits give  $(a/a_0)_{\text{P0}} = 1.0119(4)$  and  $K_0(a) = 35.9(5)$  GPa for the  $a$ -axis,  $(b/b_0)_{\text{P0}} = 1.0125(6)$  and  $K_0(b) = 34.9(7)$  GPa for the  $b$  axis, and  $(c/c_0)_{\text{P0}} = 0.9624(6)$  and  $K_0(c) = 35.5(7)$  GPa for the  $c$  axis [ $K_0(a):K_0(b):K_0(c) = 1.03:1:1.02$ ] (Fig. 2).

The crystals of leucite were recovered from the DAC after the HP experiments performed at the ESD-MI and at the BGI. The measured unit-cell constants and the reflection conditions showed a complete restoration of the tetragonal structure of leucite stable at room conditions.

## RESULTS: STRUCTURAL EVOLUTION WITH PRESSURE

The HP-crystal structure evolution of the tetragonal polymorph of leucite was studied on the basis of six structural refine-

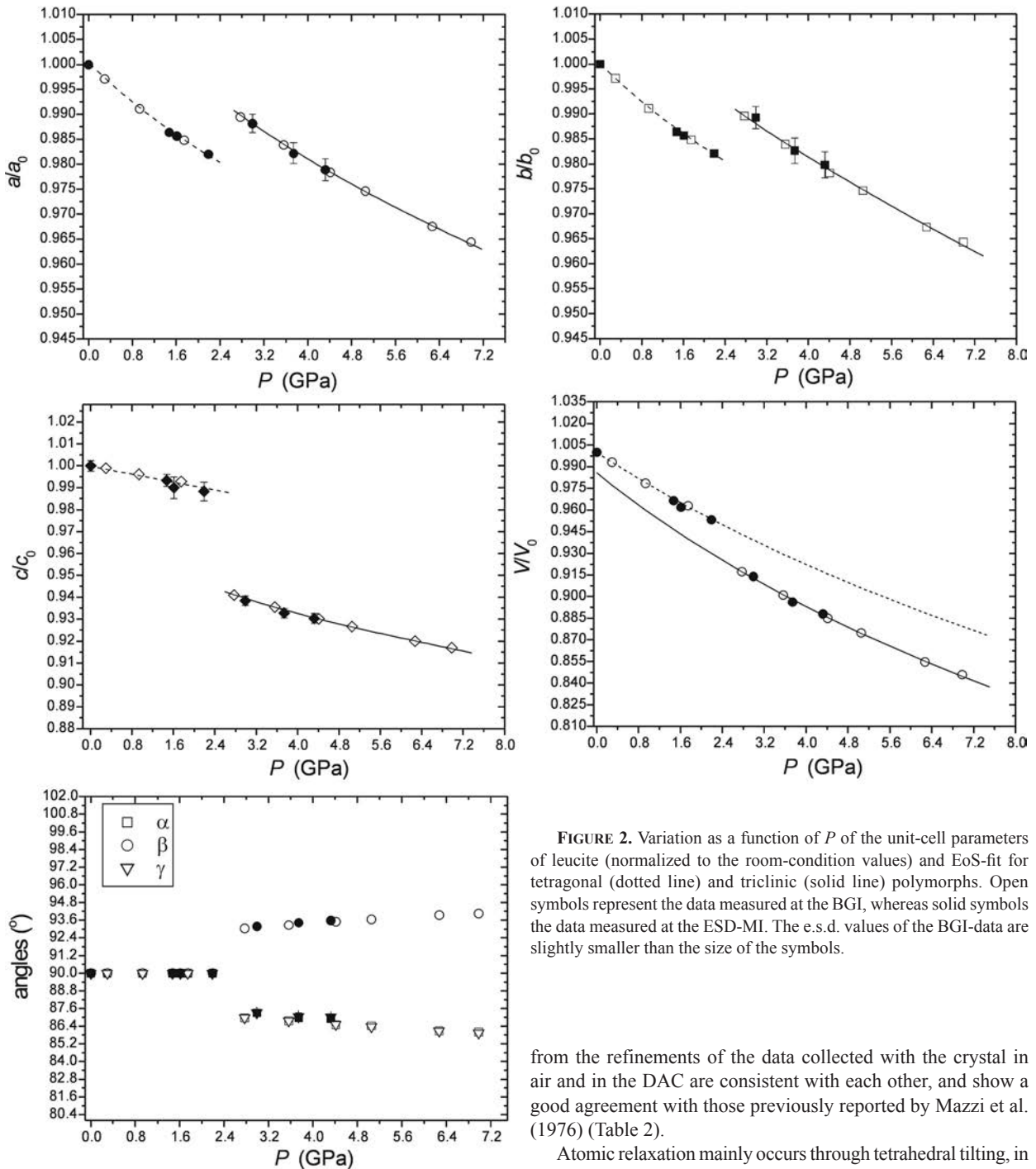


FIGURE 2. Variation as a function of  $P$  of the unit-cell parameters of leucite (normalized to the room-condition values) and EoS-fit for tetragonal (dotted line) and triclinic (solid line) polymorphs. Open symbols represent the data measured at the BGI, whereas solid symbols the data measured at the ESD-MI. The e.s.d. values of the BGI-data are slightly smaller than the size of the symbols.

ments at different pressures (Table 1): at 0.0001 (with the crystal in air); 0.0001 (with the crystal in the DAC); 0.38, 1.20, 1.77, and at 0.0001 GPa (with the crystal in air after decompression). A careful inspection of the diffraction pattern showed no violation of the reflection conditions of the space group  $I4_1/a$  within the stability field of the tetragonal polymorph (i.e., 0.0001–2.4 GPa). The framework and extra-framework site positions obtained

from the refinements of the data collected with the crystal in air and in the DAC are consistent with each other, and show a good agreement with those previously reported by Mazzi et al. (1976) (Table 2).

Atomic relaxation mainly occurs through tetrahedral tilting, in the  $P$ -range explored. The tetrahedral bond distances are practically invariant as a function of  $P$  within the stability field of the tetragonal polymorph. The only system of channels in the tetragonal leucite structure runs along  $[\bar{1}1\bar{1}]$ , with two independent six-membered rings: -T3-T3-T2-T3-T3-T2- (hereafter: 6mR-1) and -T1-T1-T2-T1-T1-T2- (hereafter: 6mR-2) (overlapped in Figure 4 with a sequence: ...6mR-1/6mR-2/6mR-1..., 6mR-2 lying on the inversion center). These two 6mRs are differently deformed (and oriented) at room conditions, with a different ellipticity ratio (Fig. 4; Table 3), 6mR-1 being more elliptic than 6mR-2. Upon

**TABLE 4.** Unit-cell parameters of leucite at different pressures, measured at the Earth Sciences Department, University of Milan (ESD-MI) and at the Bayerisches Geoinstitut (BGI)

$P$ (GPa)	$a$ (Å)	$b$ (Å)	$c$ (Å)	$\alpha$ (°)	$\beta$ (°)	$\gamma$ (°)	$V$ (Å <sup>3</sup> )
<b>Data measured at the ESD-MI</b>							
0.0001*	13.045(3)	13.045(3)	13.744(23)	90	90	90	2339(5)
1.47(3)	12.868(3)	12.868(3)	13.653(29)	90	90	90	2260(6)
1.61(5)	12.858(3)	12.858(3)	13.607(63)	90	90	90	2250(11)
2.19(4)	12.811(2)	12.811(2)	13.584(54)	90	90	90	2229(9)
2.99(7)	12.891(24)	12.905(29)	12.897(19)	87.31(21)	93.19(14)	87.31(21)	2137(12)
3.74(6)	12.813(27)	12.819(33)	12.820(21)	86.97(23)	93.43(15)	87.05(24)	2096(13)
4.32(6)	12.770(28)	12.782(34)	12.786(23)	86.91(24)	93.57(16)	87.01(24)	2077(14)
<b>Data measured at the BGI</b>							
0.0001*	13.0741(9)	13.0741(9)	13.755(1)	90	90	90	2351.1(1)
0.30(2)	13.0365(8)	13.0365(8)	13.739(1)	90	90	90	2335.0(1)
0.93(2)	12.9580(6)	12.9580(6)	13.702(1)	90	90	90	2300.7(1)
1.75(1)	12.8758(9)	12.8758(9)	13.657(1)	90	90	90	2264.1(1)
2.77(1)	12.937(1)	12.937(2)	12.943(3)	86.97(2)	93.04(1)	86.97(1)	2156.9(6)
3.56(2)	12.864(1)	12.864(3)	12.868(4)	86.77(4)	93.27(2)	86.75(2)	2118.7(9)
4.41(2)	12.791(2)	12.789(3)	12.794(4)	86.50(4)	93.50(2)	86.52(2)	2080.7(9)
5.05(3)	12.743(1)	12.743(5)	12.745(4)	86.43(5)	93.65(2)	86.36(2)	2056.8(9)
6.27(4)	12.650(1)	12.647(2)	12.654(2)	86.08(1)	93.95(1)	86.06(1)	2009.4(4)
6.98(4)	12.609(2)	12.608(6)	12.612(4)	85.99(6)	94.06(2)	85.93(4)	1989(1)

Note: Standard deviations are in parentheses.

\* Crystal in the DAC, without  $P$ -medium.

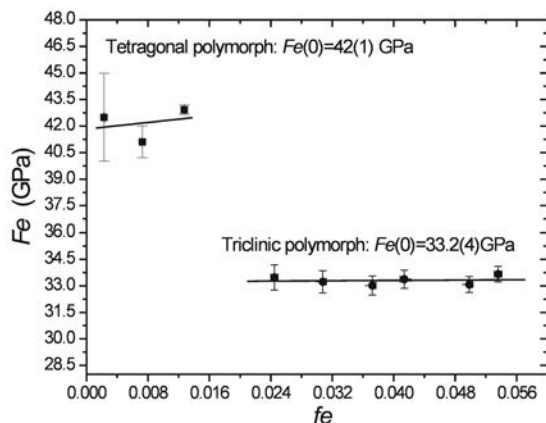


**FIGURE 3.** Plot of the Eulerian finite strain ( $f_e$ ) vs. the normalized stress ( $F_e$ ) for tetragonal and triclinic leucite. The e.s.d. values were calculated according to Angel (2000). The weighted linear regressions through the data points are shown.

increasing pressure, we observed that both rings grow more elliptic, as shown in Table 3 and Figure 5. However, 6mR-1 exhibits a drastic configuration (with  $\epsilon_{6mR-1} \approx 0.669-0.670$ ) at about 1.20 GPa, showing a saturation effect between 1.20 and 1.77 GPa (Fig. 5; Table 3), whereas 6mR-2 maintains an almost constant value of the ellipticity ratio up to 1.20 GPa (with  $\epsilon_{6mR-2} \approx 0.845-0.849$ ), followed then by a rapid decrease of  $\epsilon_{6mR-2}$  ( $\sim 0.835$ ) between 1.20 and 1.77 GPa (Fig. 5; Table 3). The compressional behavior of the 6mR-1 ring, based on an increase of ellipticity, is characterized by a contraction of the framework mainly along the  $a$  and  $b$  axes (Fig. 4). In contrast, the configuration and the deformation mechanisms of the 6mR-2 ring gives rise to a compression of the framework equally distributed along all the three axes. As a consequence, the compression of the 6mR-1 seems to govern the elastic anisotropy of the structure, as shown by the different values of  $K_0(a)$  and  $K_0(c)$ .

The further secondary building unit of the ANA-type framework is represented by the four-membered rings (4mRs,

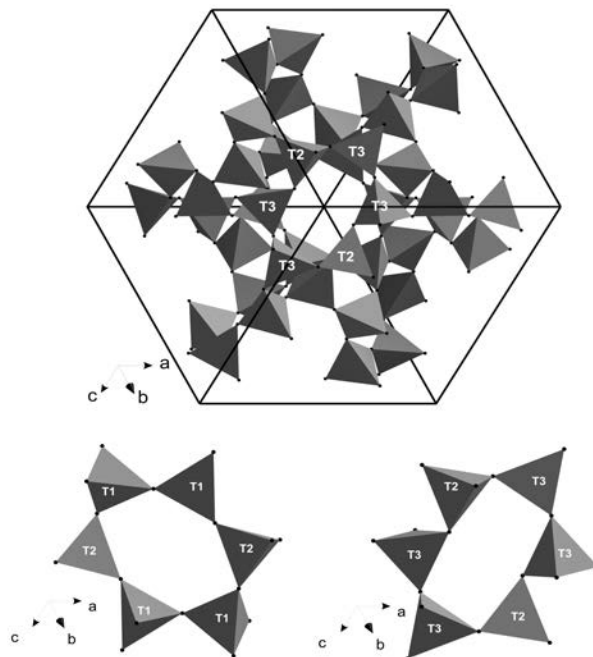


**FIGURE 4.** Configuration of the two independent 6mR rings in tetragonal leucite (i.e., 6mR-1: -T3-T3-T2-T3-T3-T2-, 6mR-2: -T1-T1-T2-T1-T1-T2-) lying along the  $[\bar{1}11]$  direction.

Baerlocher et al. 2001). In tetragonal leucite, there are three independent 4mRs: -T1-T1-T1-T1- (hereafter 4mR-1), -T3-T3-T3-T3- (hereafter 4mR-2) and -T2-T1-T2-T3- (hereafter 4mR-3). 4mR-1 and 4mR-2 behave as rigid units in the tetragonal structure at high  $P$ , because of the symmetry, they cannot deform and their ellipticity ratio is 1 at any given  $P$ . In contrast, the 4mR-3 is a deformable unit, whose ellipticity ratio  $\epsilon_{4mR-3} \approx 0.944$  at room conditions and decreases monotonically to  $\sim 0.927$  at 1.77 GPa (Fig. 5; Table 3).

The extra-framework atom does not show any relevant change within the stability field of the tetragonal polymorph, as shown

by the atomic position and thermal displacement parameter of the potassium site (Table 2). The K site in leucite is considered to be coordinated to 12 O atoms, with six K-O bond distances  $\leq 3.1$  Å and the further six distances between 3.4 and 3.8 Å (Mazzi et al. 1976). Therefore, two distinct shells of coordination can be found. We observed that for the first shell of coordination, with  $K-O < 3.14$  Å and  $CN(K) = 6$  (Table 3), no relevant change occurs with  $P$ . A change is observed to occur through the sec-

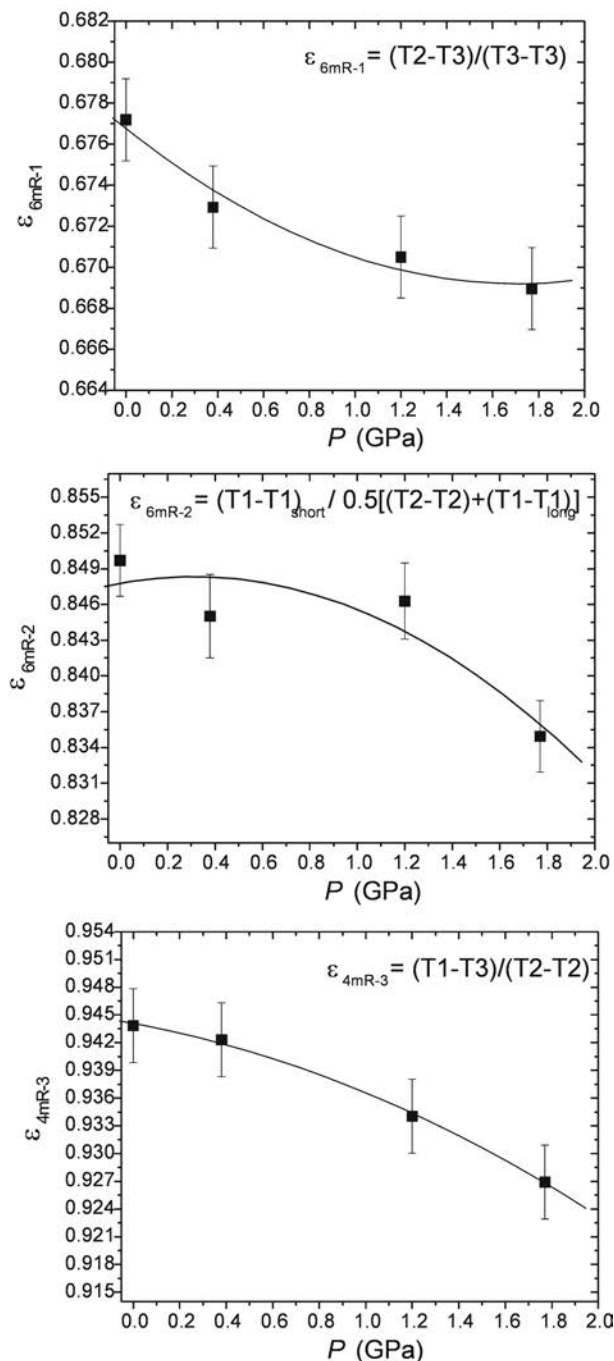


FIGURE 5. Evolution of the ellipticity ratio of the 6mR-1, 6mR-2, and 4mR-3 with  $P$ . The solid lines are drawn as guides to the eye.

ond shell of coordination, with  $K-O > 3.46$  Å (Table 3). If we consider the longest K-O bond distance to be shorter than the shortest K-Si distance (i.e.,  $\sim 3.64$  Å at 0.0001 GPa and  $\sim 3.55$  Å at 1.77 GPa), the theoretical coordination number of the potassium site is  $CN = 9$  at 0.0001 GPa and decreases with  $P$  ( $CN = 8$  at 1.20 GPa and  $CN = 7$  at 1.77 GPa) (Table 3). However, the decrease of  $CN$  with  $P$  is unusual, and supports the idea that the effective  $CN$  of the potassium site in tetragonal leucite is 6. Assuming an effective  $CN(K) = 6$  at 0.0001 GPa, we can infer that the  $CN(K)$  is maintained within the  $P$ -range investigated and the evolution of the K-O bond distances (and angles) show a homogeneous compression without any relevant distortion of the polyhedron (Table 3).

The complex  $P$ -induced twinning, due to the tetragonal  $\rightarrow$  triclinic phase-transition, and the low quality of the diffraction data at pressure above the phase-transition, did not allow the refinement of the crystal structure of the triclinic polymorph. Any attempt to refine the structure of the triclinic leucite starting with a structural model based on the tetragonal structure was unsuccessful. However, the reflection conditions suggest that the space group of the triclinic polymorph is  $P\bar{1}$ .

## DISCUSSION AND CONCLUSIONS

Leucite shows a heretofore unreported first-order phase transition at  $2.4 \pm 0.2$  GPa from the tetragonal ( $I4_1/a$ ) to the triclinic (probably  $P\bar{1}$ ) symmetry. On the basis of the HP/HT behavior of leucite, described in this study and in previous investigations at high temperature, a new schematic phase-diagram is shown in Figure 6. The tetragonal  $\rightarrow$  triclinic phase-transition at about 2.4 GPa leads to a strong distortion of the lattice, being  $\alpha \approx 86.97^\circ$ ,  $\beta \approx 93.04^\circ$ , and  $\gamma \approx 86.97^\circ$  at 2.77 GPa (Table 4). The  $P$ -induced structural evolution is described here only for the low- $P$  tetragonal polymorph, due to the impossibility of refining the structure of the high- $P$  triclinic polymorph with the present data. However, on the basis of the structural homologies with analcime, we believe that the  $P$ -induced phase-transition in leucite is displacive in character. In analcime, in fact, a first-order phase-transition from

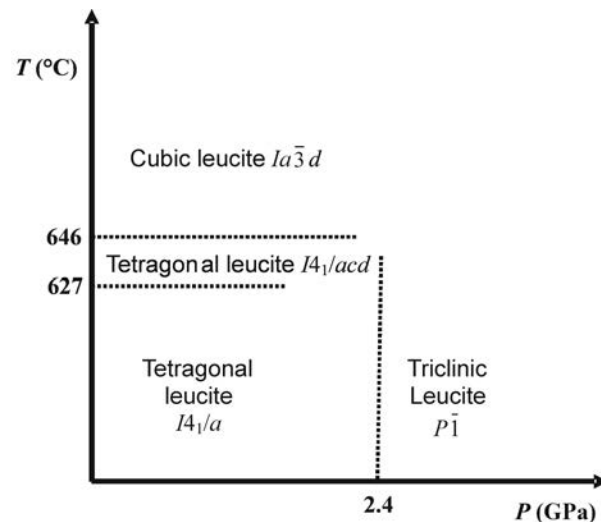


FIGURE 6. New schematic phase-diagram of leucite based on the experimental findings of this study and on previous investigations at high temperature.

the high-symmetry to the low-symmetry polymorph (i.e., cubic  $\rightarrow$  triclinic) occurs at about 1 GPa (Gatta et al. 2006; Gatta 2008). The structural refinements of the low- and high- $P$  polymorphs confirmed that the  $P$ -induced phase-transition is displacive in character, caused by simple distortion in the low- $P$  structure, which maintains the topology of the high-symmetry phase. Analcime and leucite are isotypic compounds (Baerlocher et al. 2001), topologically identical but with a different extra-framework content (K in leucite and Na + H<sub>2</sub>O in analcime). A similar HP behavior was also observed in wairakite (Ca<sub>8</sub>Al<sub>16</sub>Si<sub>32</sub>O<sub>96</sub>·16H<sub>2</sub>O, isotypic with leucite and analcime) with a phase-transition from monoclinic-to-triclinic structure at  $\sim$ 2.5 GPa (Ori et al. 2008). Therefore, the extra-framework cations seem to control the transition pressure. However, a simple relationship between ionic radius of the extra-framework cation and transition pressure does not provide an exhaustive explanation, as the configuration of the channel content among the aforementioned ANA-type zeolites is completely different [i.e., NaO<sub>4</sub>(H<sub>2</sub>O)<sub>2</sub>-polyhedron in low- $P$  analcime; KO<sub>6</sub> in low- $P$  leucite, with the K sites located at the same positions of the H<sub>2</sub>O-molecules O atoms in analcime; CaO<sub>4</sub>(H<sub>2</sub>O)<sub>2</sub>-polyhedron in low- $P$  wairakite, with a configuration similar to that of analcime].

Tetragonal leucite shows a strongly anisotropic elastic behavior, being  $K_0(c) \approx 2 \cdot K_0(a)$ , in contrast with the triclinic leucite that behaves almost isotropically, having  $K_0(a) \approx K_0(b) \approx K_0(c)$ ; this is consistent with the latter getting more stable as a function of pressure than the former. The structural evolution with pressure of the low- $P$  tetragonal polymorph of leucite is based on the deformation of the two SBUs, represented by four- and six-membered rings. In particular, the two independent 6mRs show an increase in ellipticity with  $P$ , making the structure elastically anisotropic. The ring deformations at high  $P$  follow the general principle postulated by Gatta and Lee (2006, 2007) and Gatta (2008) for open-framework silicate: the open framework structures tend to accommodate the effect of pressure, by cooperative rotation of the tetrahedra, usually increasing the ellipticity of the channel (or ring) systems and maintaining the original elliptical configuration, without any "inversion" in ellipticity. Due to the lack of structural data pertaining to the high- $P$  triclinic polymorph, the microscopic reasons of the quasi-isotropic compressibility of the triclinic leucite remain unknown. One might however assume the ellipticity to be representative of a stress propagating through the structure, giving rise to the symmetry break that causes the phase-transition. The  $P$ -induced increase in ellipticity of the 6mR-1 ring is due to tetrahedral tilting, changing the T2-O3-T2, T3-O6-T3, and T3-O5-T2 angles. At room pressure, the T2-O3-T3 angle is  $\sim$ 131.6° and decreases to  $\sim$ 126.2° at 1.77 GPa. A decrease within the same  $P$  range is also observed for the T3-O6-T3 and T3-O5-T2 angles (from  $\sim$ 130.9 to  $\sim$ 128.2° and from  $\sim$ 130.3 to  $\sim$ 127.8°, respectively). Such a decrease leads to a configuration energetically unstable at  $P > 2$  GPa, forcing the structure to reduce the symmetry to allow more degrees of freedom to the 6mR ring's deformation under compression. A similar behavior was observed in analcime at high pressure (Gatta et al. 2006).

As for analcime and wairakite, so for leucite the high- $P$  polymorph is more compressible than the low- $P$  one. However, in leucite and wairakite, the difference between the bulk moduli

of the respective polymorphs [i.e.,  $K_{0(\text{tetragonal leucite})} = 41.9(6)$  GPa and  $K_{0(\text{triclinic leucite})} = 33.2(5)$  GPa;  $K_{0(\text{monoclinic wairakite})} = 39(3)$  GPa and  $K_{0(\text{triclinic wairakite})} = 24(3)$  GPa (Ori et al. 2008)] is not so drastic as in analcime [ $K_{0(\text{cubic analcime})} = 56(3)$  GPa and  $K_{0(\text{triclinic analcime})} = 19(2)$  GPa (Gatta et al. 2006)].

As for analcime and wairakite, the  $P$ -induced structural evolution in leucite is completely reversible, despite the strong deformation of the lattice due to the tetragonal  $\rightarrow$  triclinic phase transition. In addition, we observed that the complex twinning associated to the HP phase transition in leucite does not hamper the complete reversibility of the triclinic  $\rightarrow$  tetragonal reverse transformation in decompression, as shown by the structural refinement based on data collected with the crystal in air after the HP experiments.

Leucite is one of the main components of alkaline ultrapotassic rocks. In their study on the HP-transformation of K-rich framework silicates (i.e., sanidine, leucite, and kalsilite), Ringwood et al. (1967) showed that at 12 GPa and 900 °C leucite disproportionates into hollandite and a further K-rich phase by the following reaction:



A similar behavior was observed, under the same conditions, for sanidine. In contrast, kalsilite appeared to be stable, without any transformation to hollandite. However, a further reinvestigation of the HP-HT transformations of potassium aluminosilicates performed by Liu (1987) showed that sanidine and leucite transform to K<sub>2</sub>Si<sub>4</sub>O<sub>9</sub> wadeite-type phase (+ kyanite + coesite) in the vicinity of 5 GPa and 1000 °C. And at  $P > 17$  GPa, hollandite + KAlO<sub>2</sub> are the only stable K-rich phases. On the basis of the most recent data reported by Liu (1987), it appears that leucite is a stable phase at upper-mantle conditions at least up to 4–5 GPa (at 1000 °C) and can be considered an appropriate host for K in anhydrous iper-alkaline systems. In K-rich hydrous systems, phlogopite can be considered as a possible host for K. Therefore, the  $P$ -induced first-order phase-transition observed in this study at about 2.4 GPa, with a drastic increase in density ( $\sim$ 4.7%) and a change in the elastic behavior, should be taken into account for geophysical and geological interpretations of anhydrous K-rich petrogenetic systems stable at such  $P$ - $T$  conditions.

## ACKNOWLEDGMENTS

High-pressure experiments at the Bayerisches Geoinstitut were performed under the EU "Research Infrastructures: Transnational Access" Program [contract no. 505320 (RITA)-High Pressure]. This work was also funded by the Italian Ministry of University and Research, MIUR-Project: 2006040119\_004 (grant to A. Pavese). The authors thank Angelo Peccerillo for his fruitful suggestions. The Associate Editor P. Dera and two anonymous reviewers are thanked for the revision of the manuscript.

## REFERENCES CITED

- Angel, R.J. (2000) Equation of state. In R.M. Hazen and R.T. Downs, Eds., *High-temperature and High-pressure Crystal Chemistry*, 41, p. 35–59. Reviews in Mineralogy and Geochemistry, Mineralogical Society of America, Chantilly, Virginia.
- (2001) EOS-FIT V6.0. Computer program. Crystallography Laboratory, Department Geological Sciences, Virginia Tech, Blacksburg, Virginia.
- (2002) ABSORB V5.2. Computer program. Crystallography Laboratory, Department Geological Sciences, Virginia Tech, Blacksburg, Virginia.
- (2003) Automated profile analysis for single-crystal diffraction data. *Journal of Applied Crystallography*, 36, 295–300.
- Angel, R.J., Allan, D.R., Miletich, R., and Finger, L.W. (1997) The use of quartz as

- an internal pressure standard in high-pressure crystallography. *Journal of Applied Crystallography*, 30, 461–466.
- Angel, R.J., Downs, R.T., and Finger, L.W. (2000) High-temperature–High-pressure diffraction. In R.M. Hazen and R.T. Downs, Eds., *High-temperature and High-pressure Crystal Chemistry*, 41, p. 559–596. Reviews in Mineralogy and Geochemistry, Mineralogical Society of America, Chantilly, Virginia.
- Angel, R.J., Bujak, M., Zhao, J., Gatta, G.D., and Jacobsen, S.D. (2007) Effective hydrostatic limits of pressure media for high-pressure crystallographic studies. *Journal of Applied Crystallography*, 40, 26–32.
- Armbruster, T. and Gunter, M.E. (2001) Crystal structures of natural zeolites. In D.L. Bish and D.W. Ming, Eds., *Natural Zeolites: Occurrence, Properties, Application*, 45, p. 1–57. Reviews in Mineralogy and Geochemistry, Mineralogical Society of America, Chantilly, Virginia.
- Baerlocher, Ch., Meier, W.M., and Olson, D.H. (2001) *Atlas of Zeolite Framework Types*, 5th edition, 302 p. Elsevier, Amsterdam.
- Birch, F. (1947) Finite elastic strain of cubic crystals. *Physical Review*, 71, 809–824.
- Boysen, H. (1990) Neutron scattering and phase transitions in leucite. In E.K.H. Salje, Ed., *Phase transitions in ferroelastic and co-elastic materials*, p. 334–349. Cambridge University Press, U.K.
- Brown, I.W.M., Cardile, C.M., Mackenzie, K.J.D., Ryan, M.J., and Meinhold, R.H. (1987) Natural and synthetic leucites studied by solid state 29-Si NMR and 27-Al NMR and 57-Fe Mössbauer spectroscopy. *Physics and Chemistry of Minerals*, 15, 78–83.
- Burnham, C.W. (1966) Computation of absorption corrections and the significance of end effect. *American Mineralogist*, 51, 159–167.
- Coombs, D.S., Alberti, A., Armbruster, T., Artioli, G., Colella, C., Galli, E., Grice, J.D., Liebau, F., Mandarino, J.A., Minato, H., Nickel, E.H., Passaglia, E., Peacor, D.R., Quartieri, S., Rinaldi, R., Ross, M., Sheppard, R.A., Tillmanns, E., and Vezzolini, G. (1997) Recommended nomenclature for zeolite minerals: Report of the Subcommittee on Zeolites of International Mineralogical Association, Commission on new minerals and minerals names. *Canadian Mineralogist*, 35, 1571–1606.
- Coticelli, S. and Peccerillo, A. (1992) Petrology and geochemistry of potassic and ultrapotassic volcanism in Central Italy: Petrogenesis and inferences on the evolution of the mantle sources. *Lithos*, 28, 221–240.
- Coticelli, S., D'Antonio, M., Pinarelli, L., and Civetta, L. (2002) Source contamination and mantle heterogeneity in the genesis of Italian potassic and ultrapotassic volcanic rocks: Sr-Nd-Pb isotope data from Roman Province and Southern Tuscany. *Mineralogy and Petrology*, 74, 189–222.
- Deer, W.A., Howie, R.A., and Zussman, J. (2004) *Rock-forming minerals*, Vol. 4B: Framework silicates. The Geological Society, London, U.K.
- Dove, M.T., Cool, T., Palmer, D.C., Putnis, A., Salje, E.K.H., and Winkler, B. (1993) On the role of Al-Si ordering in the cubic-tetragonal phase transition in leucite. *American Mineralogist*, 78, 486–492.
- Fasshauer, D.W., Wunder, B., Chatterjee, N.D., and Höhne, G.W.H. (1998) Heat capacity of wadeite-type  $K_2Si_4O_{13}$  and the pressure-induced stable decomposition of K-feldspar. *Contributions to Mineralogy and Petrology*, 131, 210–218.
- Faust, G.T. (1963) Phase transition in synthetic and natural leucite. *Schweizerische Mineralogische und Petrographische Mitteilungen*, 43, 165–195.
- Federico, M., Peccerillo, A., Barbieri, M., and Wu, T.W. (1994) Mineralogical and geochemical study of granular xenoliths from the Alban Hill volcano, central Italy: Bearing on evolutionary processes in potassic magma chambers. *Contributions to Mineralogy and Petrology*, 115, 384–401.
- Gatta, G.D. (2008) Does porous mean soft? On the elastic behavior and structural evolution of zeolites under pressure. *Zeitschrift für Kristallographie*, 223, 160–170.
- Gatta, G.D. and Lee, Y. (2006) On the elastic behavior of zeolite mordenite: A synchrotron powder diffraction study. *Physics and Chemistry of Minerals*, 32, 726–732.
- (2007) Anisotropic elastic behavior and structural evolution of zeolite phillipsite at high-pressure: A synchrotron powder diffraction study. *Microporous and Mesoporous Materials*, 105, 239–250.
- Gatta, G.D., Nestola, F., and Boffa Ballaran, T. (2006) Elastic behavior, phase transition, and pressure induced structural evolution of analcime. *American Mineralogist*, 91, 568–578.
- Gottardi, G. and Galli, E. (1985) *Natural Zeolites*, 409 p. Springer-Verlag, Berlin.
- Hatch, D.M., Ghose, S., and Stokes, H.T. (1990) Phase transitions in leucite,  $KAlSi_3O_8$ . *Physics and Chemistry of Minerals*, 17, 220–227.
- Heaney, P.J. and Veblen, D.R. (1990) A high-temperature study of the low–high leucite phase transition using the transmission electron microscope. *American Mineralogist*, 75, 464–476.
- Hirao, K., Soga, N., and Kunugi, M. (1976) Thermal expansion and structure of leucite-type compounds. *Journal of Physical Chemistry*, 80, 1612–1616.
- King, H.E. and Finger, L.W. (1979) Diffracted beam crystal centering and its application to high-pressure crystallography. *Journal of Applied Crystallography*, 12, 374–378.
- Lange, R.A., Carmichael, I.S.E., and Stebbins, J.F. (1986) Phase transitions in leucite ( $KAlSi_3O_8$ ), orthorhombic  $KAlSiO_4$ , and their iron analogues ( $KFeSi_3O_8$ ,  $KFeSiO_4$ ). *American Mineralogist*, 71, 937–945.
- Liu, L. (1987) High-pressure phase transitions of potassium aluminosilicates with an emphasis on leucite. *Contributions to Mineralogy and Petrology*, 95, 1–3.
- Mazzi, F., Galli, E., and Gottardi, G. (1976) The crystal structure of tetragonal leucite. *American Mineralogist*, 61, 108–115.
- Miletich, R., Allan, D.R., and Kush, W.F. (2000) High-pressure single-crystal techniques. In R.M. Hazen and R.T. Downs, Eds., *High-temperature and High-pressure Crystal Chemistry*, 41, p. 445–519. Reviews in Mineralogy and Geochemistry, Mineralogical Society of America, Chantilly, Virginia.
- Murnaghan, F.D. (1937) Finite deformations of an elastic solid. *American Journal of Mathematics*, 49, 235–260.
- Newton, H., Hayward, S.A., and Redfern, S.A.T. (2008) Order parameter coupling in leucite: a calorimetric study. *Physics and Chemistry of Minerals*, 35, 11–16. DOI: 10.1007/s00269-007-0193-3.
- Ori, S., Quartieri, S., Vezzolini, G., and Dmitriev, V. (2008) Pressure-induced structural deformation and elastic behavior of wairakite. *American Mineralogist*, 93, 53–62.
- Oxford Diffraction (2005) *CrysAlis Software system*, Version 1.170. Xcalibur CCD system, Oxford Diffraction Ltd.
- Palmer, D.C., Putnis, A., and Salje, E.K.H. (1988) Twinning in tetragonal leucite. *Physics and Chemistry of Minerals*, 16, 298–303.
- Palmer, D.C., Salje, E.K.H., and Schmahl, W.W. (1989) Phase transitions in leucite: X-ray diffraction studies. *Physics and Chemistry of Minerals*, 16, 714–719.
- Palmer, D.C., Bismayer, U., and Salje, E.K.H. (1990) Phase transitions in leucite: Order parameter behavior and the Landau potential deduced from Raman spectroscopy and birefringence studies. *Physics and Chemistry of Minerals*, 17, 259–265.
- Palmer, D.C., Dove, M.T., Ibberson, R.M., and Powell, B.M. (1997) Structural behavior, crystal chemistry, and phase transitions in substituted leucite: High-resolution neutron powder diffraction studies. *American Mineralogist*, 82, 16–29.
- Peacor, D.R. (1968) A high-temperature single-crystal diffractometer study of leucite,  $(K, Na)AlSi_3O_8$ . *Zeitschrift für Kristallographie*, 127, 213–224.
- Peccerillo, A. (1998) Relationships between ultrapotassic and carbonate-rich volcanic rocks in central Italy: Petrogenetic and geodynamic implications. *Lithos*, 43, 267–279.
- (2003) Plio-Quaternary magmatism in Italy. *Episodes*, 26, 222–226.
- (2005) Plio-Quaternary volcanism in Italy: Petrology, Geochemistry, Geodynamics, 365 p. Springer, Heidelberg.
- Ringwood, A.E., Reid, A.F., and Wadsley, A.D. (1967) High-pressure  $KAlSi_3O_8$ , an aluminosilicate with sixfold coordination. *Acta Crystallographica*, 23, 1093–1095.
- Sheldrick, G.M. (1997) *SHELX-97*. Programs for crystal structure determination and refinement. University of Göttingen, Germany.
- Taylor, D. and Henderson, C.M.B. (1968) The thermal expansion of the leucite group of minerals. *American Mineralogist*, 53, 1476–1489.
- Wilson, A.J.C. and Prince, E. (1999) *International tables for X-ray crystallography*, Volume C: Mathematical, physical, and chemical tables, 2nd edition. Kluwer Academic, Dordrecht.

MANUSCRIPT RECEIVED JANUARY 16, 2008

MANUSCRIPT ACCEPTED APRIL 28, 2008

MANUSCRIPT HANDLED BY PRZEMYSŁAW DERA